**Article**

# Synaptic Potential and Plasticity of an SK2 Channel Gate Regulate Spike Burst Activity in Cerebellar Purkinje Cells



Synaptic input:
connectivity map / driver

$w_1$

$w_N$

Intrinsic excitability:
efficient control of spike output

20mV

100ms

Gen Ohtsuki,
Christian Hansel

chansel@bsd.uchicago.edu

**HIGHLIGHTS**

The study is based on somato-dendritic double-patch recordings from Purkinje cells

Dendritically recorded EPSP amplitudes predict the occurrence of spike firing

Synaptic weight does not predict whether individual spikes or spike bursts occur

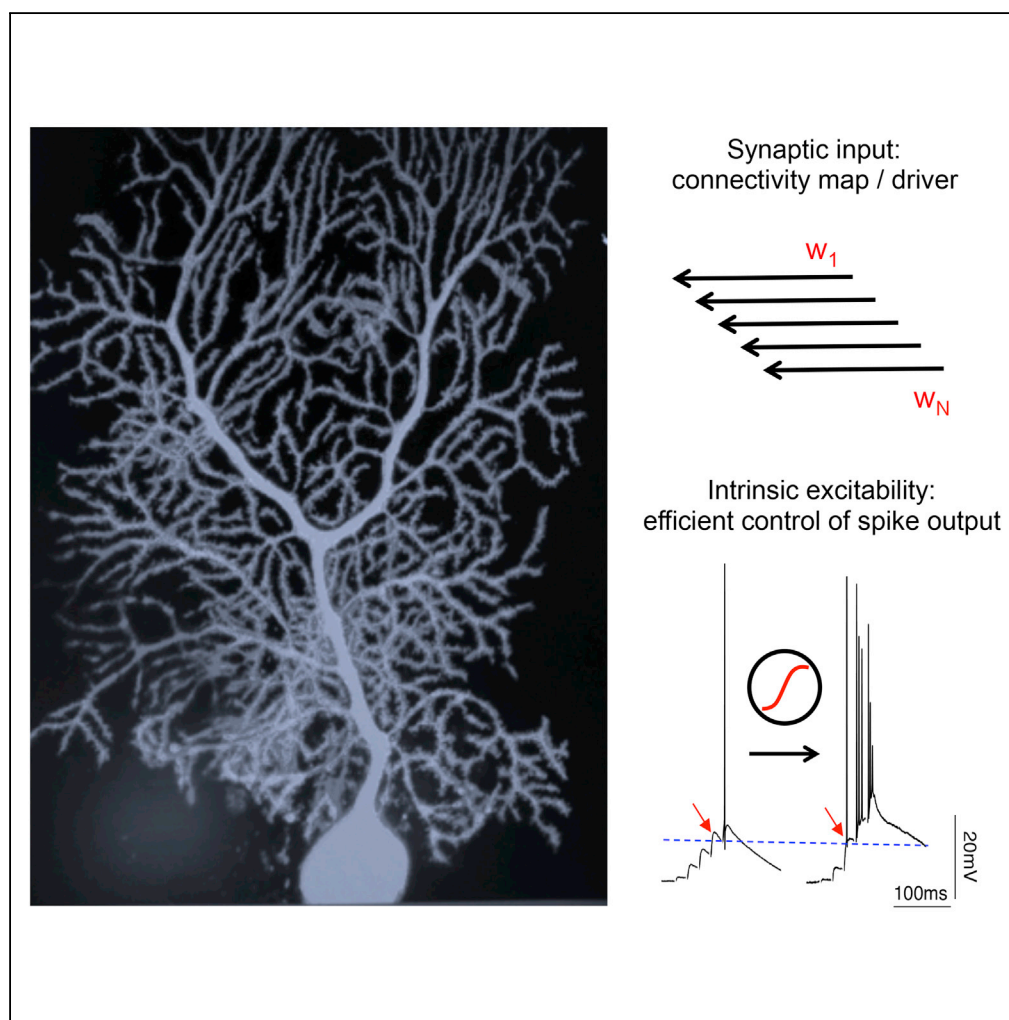SK2 channel modulation/plasticity efficiently controls the spike output

# iScience

## Article

# Synaptic Potential and Plasticity of an SK2 Channel Gate Regulate Spike Burst Activity in Cerebellar Purkinje Cells

Gen Ohtsuki[1,2,3] and Christian Hansel[1,4,*]

## SUMMARY

**Neurons store information and participate in memory engrams as a result of experience-dependent changes in synaptic weights and in membrane excitability. Here, we examine excitatory postsynaptic potential (EPSP) amplitude and neuronal excitability in relation to these two mechanisms of plasticity. We analyze somato-dendritic double-patch recordings from cerebellar Purkinje cells while inducing intrinsic, SK2 channel-dependent plasticity or blocking SK channels with bath application of apamin. Both manipulations increase the build-up of EPSP amplitudes during an EPSP train and enhance the number of EPSP-evoked spikes, yielding insights into the mechanistic contribution of EPSP amplitude to single spikes and spike bursts. EPSP amplitude has an impact on whether spikes are fired or not, but direct measures of excitability (spike threshold/AHP) are better predictors of whether individual spikes or spike bursts are fired. Our findings show that Purkinje cell spiking is synaptically driven but that burst firing is gated by SK2 channel modulation and plasticity.**

## INTRODUCTION

It has previously been argued that changes in the intrinsic excitability of neurons ("intrinsic plasticity") may provide a second group of plasticity phenomena that play a role in learning—independent from synaptic plasticity (e.g., long-term potentiation; LTP) or complementing it (Marder et al., 1996; Hansel et al., 2001). In further development of an "intrinsic theory" of learning, we have recently hypothesized that synaptic plasticity primarily establishes connectivity patterns between neurons, whereas intrinsic plasticity provides the main mechanism for the integration of neurons into active engrams (Titley et al., 2017; see also Piochon et al., 2016). A prediction from this hypothesis is that in some types of neurons, particularly in neurons with long primary dendrites, such as layer V pyramidal neurons, synaptic weight is a poor predictor of the spike outcome. Purkinje cells do have relatively short primary dendrites (in rodents, the molecular layer is ~150–200 μm thick; e.g., Piochon et al., 2014) that, however, show a high degree of branching. The complex dendritic geometry (Vetter et al., 2001) and the low density of specific $Na^+$ channel α-subunits ($Na_v1.1$ channel; De Ruiter et al., 2006) are seen as factors contributing to the absence of $Na^+$ spike backpropagation into Purkinje cell dendrites (Stuart and Häusser, 1994). A consequence of the shortness of the dendrite, combined with the low $Na^+$ channel density and the lack of spike backpropagation is that these dendrites are electronically compact, which reduces the impact of attenuating factors on the excitatory postsynaptic potential (EPSP) amplitude (Roth and Häusser, 2001). Purkinje cells, however, face the challenge that burst firing is needed to transiently override the high spontaneous discharge activity (up to 150 Hz; Häusser and Clark, 1997) to influence spike firing in target neurons in the cerebellar nuclei (Aizenman and Linden, 1999). We therefore analyzed somato-dendritic double-patch recordings from rat Purkinje cells, in which spike and spike burst activity were enhanced by SK2 channel modulation/plasticity, thereby exploring the impact of increased EPSP amplitude and excitability on neuronal burst firing.

## RESULTS

Double-patch recordings were obtained from Purkinje cells in young adult (P25-37) Sprague-Dawley rats at near-physiological temperature (31–34°C). Dendritic recordings were performed at 3 distances of 50–140 mm from the soma (average: 91.3 ± 4.8 mm, n=18; Figure 1A; Data S1). At both the dendritic and somatic recording site a negative bias current was injected (100–350 pA) to stabilize the membrane potential below the threshold for spontaneous spike activity, in the range of −70 to −80 mV. To assess the effect of SK2 channel plasticity on spike firing, we used previously established intrinsic plasticity protocols or bath-applied the SK channel blocker apamin (Belmeguenai et al., 2010; see also Sourdet et al.,

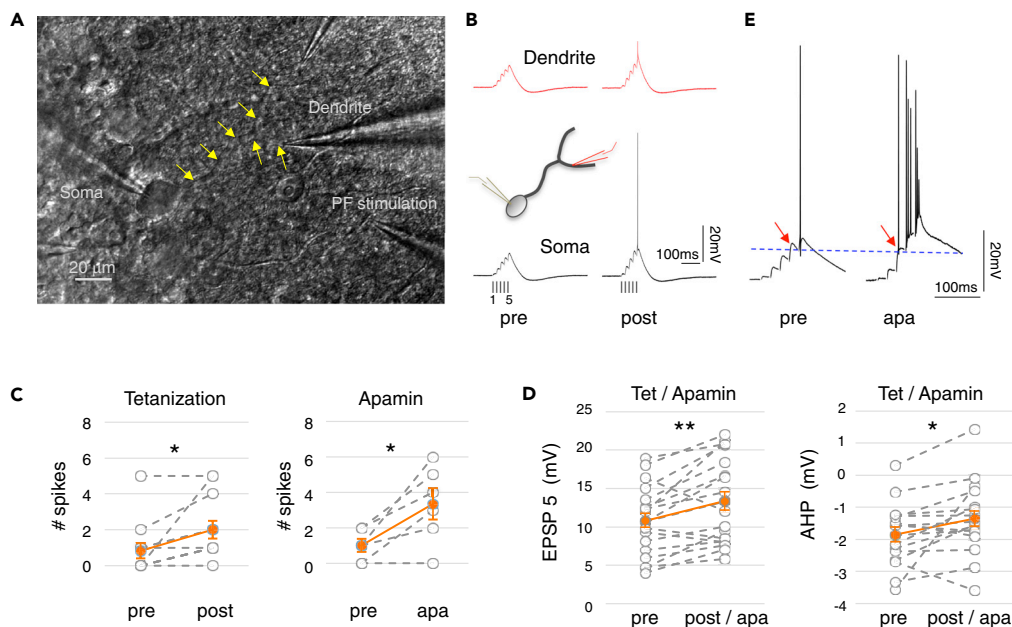[1]Department of Neurobiology, University of Chicago, Chicago, USA

[2]The Habuki Center for Advanced Research, Kyoto University, Kyoto, Japan

[3]Department of Biophysics, Kyoto University Graduate School of Science, Kyoto, Japan

[4]Lead Contact

*Correspondence: chansel@bsd.uchicago.edu

https://doi.org/10.1016/j.isci.2018.02.001

**Figure 1. The Spike Output of Purkinje Cells Changes after Tetanization or Bath Application of Apamin**

(A) Differential interference contrast (DIC) image illustrating the somato-dendritic patch-clamp configuration. Glass pipettes are used for recordings from the soma (left) and the dendrite (right; here a double dendrite recording is shown) as well as for PF stimulation (lower right). The yellow arrows point out the course of the primary dendrite.

(B) Somato-dendritic double-patch recording showing the emergence of spike firing (EPSP 5) after application of the somatic depolarization protocol. The dendritic recording was obtained at a distance of ∼98 μm from the soma. The traces were collected in response to five PF stimuli (indicated below the traces) during the baseline (pre) and 20 min after tetanization (post). The schematic depicts the somato-dendritic recording configuration shown in (A).

(C) The number of spikes evoked by stimulus 5 is enhanced after tetanization (n = 12; note that several data points overlap in their pre/post values; left) as well as after bath application of apamin (10 nM; n = 6; right). Colored symbols show means and SEM.

(D) The amplitude of the dendritically recorded EPSP 5 is enhanced after tetanization/apamin (n = 18; left). The AHP amplitude is reduced after tetanization/apamin (n = 16; right). All data shown in (C) and (D) were obtained from traces recorded during the baseline and >20 min after tetanization/apamin.

(E) Example of a somatic recording showing that in the presence of apamin spikes were evoked by EPSPs (EPSP 3 in apa) that were smaller in amplitude than larger EPSPs recorded during the baseline that did not evoke spikes (EPSP 4 in pre; arrows).

Error bars indicate SEM. *p < 0.05; **p < 0.01.

2003). Intrinsic plasticity was evoked by injection of depolarizing currents into the soma (300–400 pA/ 100 ms) or activation of parallel fiber (PF) bursts at 50 Hz (5 pulses). In both protocols, these stimuli were applied at 5 Hz for 3–4 s (n = 12).

As previously demonstrated, these protocols enhance excitability by downregulation of small-conductance, calcium-dependent SK2-type potassium channels (Belmeguenai et al., 2010; Grasselli et al., 2016). To directly assess the effects of SK channel downregulation, we also analyzed experiments in which apamin (10 nM) was applied to the bath (n = 6). In the test periods before and after tetanization or apamin wash-in, we applied five stimuli at 50 Hz to the PF input (20-s intervals). These stimuli mimic temporal summation—a potential mechanism for enhancing the impact of synaptic input—by eliciting EPSP trains of increasing amplitude (Figure 1B). Our analysis focuses on EPSP 5, which typically depolarizes the membrane sufficiently to reach the spike threshold range (see Transparent Methods). In none of these experiments did we observe a significant difference in the amplitude of dendritically recorded EPSPs (EPSP 5) and somatically recorded potentials during the baseline (dendrite: 10.76 ± 1.07 mV; soma: 10.29 ± 0.74 mV; p = 0.5429; n = 18). Thus, in the relatively short primary dendrites of cerebellar Purkinje cells we do not see the large attenuation/amplification effects during propagation of EPSPs toward the soma that have been reported for layer V pyramidal cells (Larkum et al., 2001). In the following, we base our calculation of EPSP amplitudes on the dendritic recordings to obtain more accurate measures

that are, owing to the lack of spike backpropagation in Purkinje cell dendrites (Stuart and Häusser, 1994), less confounded by spike activity than somatic measures, particularly at distances ≥80 μm from the soma (Ohtsuki et al., 2012).

Application of the 5-Hz tetanization protocol (depolarization or synaptic activation) enhanced the average spike number triggered by EPSP 5 (pre: 0.83 ± 0.42 spikes; post: 2.0 ± 0.49 spikes; p = 0.012; n = 12; Figures 1B and 1C). The same effect was observed after bath application of apamin (pre: 1.0 ± 0.36; post: 3.33 ± 0.88; p = 0.022; n = 6; Figure 1C). As 5-Hz tetanization enhances excitability as a result of a downregulation of SK channels (Belmeguenai et al., 2010; Grasselli et al., 2016), which is similarly achieved by application of the SK channel blocker apamin, the two datasets were merged for the following analysis. To determine the cause for the enhanced spike rate, we measured the amplitude of dendritically recorded EPSPs and local AHPs before and after tetanization/apamin. We observed that the EPSP amplitude was significantly enhanced (pre: 10.76 ± 1.07 mV; post: 13.37 ± 1.31 mV; n = 18; p = 0.002; Figure 1D) without accompanying changes in the resting membrane potential (pre: −75.6 ± 0.94 mV; post: −76.1 ± 0.68 mV; n = 18; p = 0.678). This increase in the EPSP amplitude may result from an LTP mechanism that can be co-induced with intrinsic plasticity (Belmeguenai et al., 2010), but it may also be a direct result of enhanced excitability. Indeed, the amplitude of EPSP 1 was not significantly changed (1.15 ± 0.27 mV; post: 1.31 ± 0.26 mV; n = 18; p = 0.245; data not shown). This observation suggests that LTP did not occur (LTP would be expected to change the amplitude of EPSP 1 regardless of the initial amplitude). Thus, it is likely that increased excitability at least partially contributes to the increase in EPSP 5, potentially in concert with other factors, such as short-term plasticity.

The dendritically recorded AHP was significantly reduced after tetanization/apamin (pre: −1.85 ± 0.25 mV; post: −1.35 ± 0.29 mV; n = 16; p = 0.045; Figure 1D), which matches the known dendritic localization of SK2 channels in Purkinje cells (Belmeguenai et al., 2010; Hosy et al., 2011; note that, of the three types of SK channel subunits, Purkinje cells express only SK2 channels; Cingolani et al., 2002) and the participation of SK conductances in the AHPs following trains of input (Edgerton and Reinhart, 2003; Womack and Khodakhah, 2003). These data identify both the EPSP amplitude and intrinsic excitability as potential contributors to the enhanced spike output following tetanization/apamin. Remarkably, we observed that, in 5 of the 16 Purkinje cells that showed spike activity during PF-EPSP trains, higher spike numbers (1 vs 0, or >1 vs 1) resulted after tetanization/apamin from EPSPs that were smaller in amplitude than the less efficient baseline EPSPs (for an example, see Figure 1E), pointing toward a limited role of the EPSP amplitude in determining the spike output.

To obtain better access to details of the spike output pattern, we analyzed individual sweeps regardless of experimental history (tetanization/apamin application) and sorted them into groups in which no spike was evoked by EPSP 5 or one, two, or more than two (3–6) spikes were evoked. Over the entire range of recordings, there was a monotonic relationship between the EPSP 5 amplitude and spike activity (Spearman's rank correlation coefficient ρ = 0.45; p = 0.00568; n = 36), suggesting that the EPSP amplitude build-up provides an efficient drive for spike generation (Figure 2A). However, a comparison of EPSP amplitudes between specific spike output groups revealed a more complex picture. When no spike was evoked, the amplitude of EPSP 5 was significantly lower than in traces where one or more spikes were evoked (0 spikes: 8.27 ± 1.07 mV, n = 11; ≥1 spike: 13.73 ± 0.96 mV, n = 25; p = 0.023). The EPSP amplitude did not predict, however, whether one or more spikes were evoked (1 spike: 13.33 ± 1.51 mV, n = 11; >1 spikes: 14.05 ± 1.22 mV, n = 14; p = 0.764; for all sweeps, in which ≥1 spike was fired: Spearman's ρ = 0.05, p = 0.7990, n = 25) or whether more than two spikes were evoked rather than one or two spikes (1–2 spikes: 13.63 ± 1.11 mV, n = 17; >2 spikes: 13.94 ± 1.84 mV, n = 8; p = 0.928; Figure 2A).

Next, we asked the question whether measures of excitability are better predictors of the spike output pattern. We found a monotonic relationship between the AHP amplitude and the spike output for sweeps with 0–2 spikes (Spearman's ρ = −0.47; p = 0.0156; n = 26), but no such relationship when sweeps with strong bursts (3–6 spikes) were included (Spearman's ρ = −0.03; p = 0.8744; n = 33). In fact, a low AHP amplitude distinguished sweeps with strong burst activity from those with one or two spikes (>2 spikes: −0.85 ± 0.42 mV, n = 7; 1–2 spikes: −2.21 ± 0.24 mV, n = 16; p = 0.049; Figure 2B). These findings are in line with the fact that calcium-dependent $K^+$ conductances underlying the AHP require calcium influx for activation (hence the increase in AHP amplitude with the emergence of spike

**A** EPSP amplitude
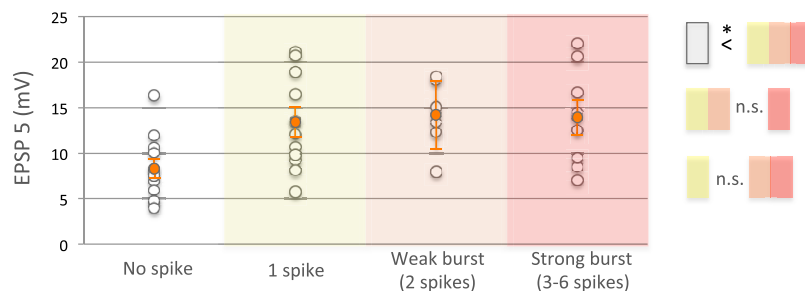


**B** Intrinsic excitability
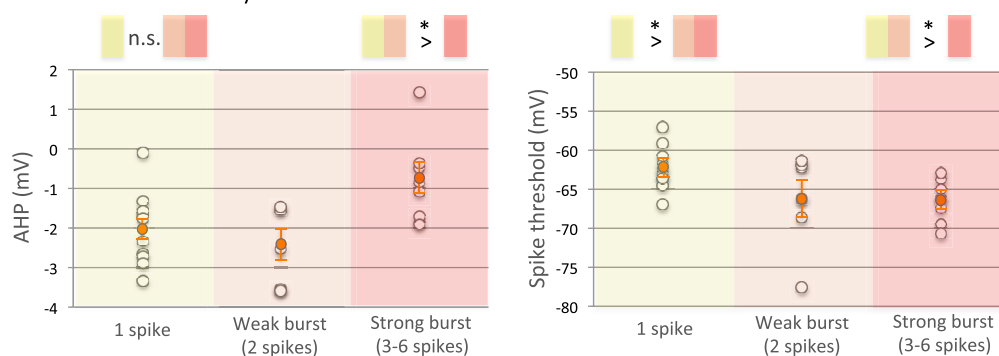


**Figure 2. EPSP Amplitude and Intrinsic Excitability as Predictors of Spike and Spike Burst Firing**

(A) Plot of the spike output versus the amplitude of EPSP 5. The spike output was categorized into four groups: no spike (n = 11), one spike (n = 11), weak burst (2 spikes; n = 6), and strong burst (3–6 spikes; n = 8). These groups are color coded to illustrate the strength of spike output.

(B) Excitability measures. As the spike threshold measure could be performed only when spiking occurred, the "no spike" group is not included. Left: Plot of the spike output versus the AHP amplitude: one spike (n = 10), weak burst (n = 6), and strong burst (n = 7). Right: Plot of the spike output versus the membrane potential at which anywhere in the EPSP train the first spike was fired (an approximation of the spike threshold): one spike (n = 10), weak burst (n = 6), and strong burst (n = 8).

Error bars indicate SEM. *p < 0.05. The colored boxes indicate the groups from which recordings were included for statistical comparison.

firing) while at the same time reflecting the permissive function of AHP modulation for strong burst firing (e.g., SK2 plasticity/blockade prevents full activation under strong calcium influx conditions and enables burst firing). Thus, when spike firing is evoked, a low AHP amplitude becomes predictive of strong burst activity.

As a second measure of excitability, we monitored the membrane potential at which the first spike was elicited within the EPSP train, which constitutes an approximation of the spike threshold. This threshold was significantly lower (more negative) when >1 spike was triggered than when one spike was evoked (1 spike: −62.33 ± 0.84 mV, n = 10; >1 spike: −66.38 ± 1.11 mV, n = 14; p = 0.021), and it was lower when more than two spikes were evoked rather than one or two spikes (1–2 spikes: −63.82 ± 1.12 mV, n = 16; >2 spikes: −66.45 mV ± 0.88 mV, n = 8; p = 0.03; Figure 2B). Measured for all recordings, in which spike activity occurred at all (n = 25), there was a monotonic relationship between the spike threshold and the spike outcome (Spearman's ρ = −0.53; p = 0.0075).

## DISCUSSION

The central finding of this study is that the EPSP amplitude shows no relation to the type of spike firing output that is generated by Purkinje cells. Instead, whether individual spikes or spike bursts are fired depends on the modulatory state of SK2 channels. From a mechanistic perspective, a prediction resulting from this observation is that learning/plasticity-related changes in EPSP amplitude (as in LTP) will be less efficient in driving spike burst firing than activity-dependent SK2 channel plasticity, a phenomenon that

we have previously described in Purkinje cells (Belmeguenai et al., 2010; Ohtsuki et al., 2012; Grasselli et al., 2016). Our findings are in line with the hypothesis that synaptic plasticity largely plays a role in establishing synaptic connectivity maps, whereas non-synaptic plasticity regulates spike firing in neurons (Titley et al., 2017).

Spike bursts are a particularly relevant output signal of Purkinje cells as they efficiently initiate hyper-polarization in cerebellar nuclei neurons, which may drive rebound activity and spike firing (for discussion, see Aizenman and Linden, 1999; Telgkamp and Raman, 2002; Alvina et al., 2008; Person and Raman, 2012; Dykstra et al., 2016). In contrast, the addition or removal of individual spikes is likely to remain inconsequential for signal propagation from the cerebellar cortex to the nuclei. The particularly low AHP values ($-0.85$ mV on average) measured when 3–6 spikes were evoked, in addition to the observation that in all but one cell these bursts emerged after SK2 channel-dependent intrinsic plasticity, or application of the SK channel blocker apamin, suggest that burst firing is gated by a downregulation of SK channels. A similar gating function of calcium-dependent $K^+$ conductances has been predicted based on studies of a realistic Purkinje cell computer model (De Schutter, 1998; note that in hippocampal CA2 pyramidal neurons gating by dendritic $Na^+$ spikes has been observed; Sun et al., 2014). Our findings provide experimental support for this suggestion. A scenario emerges in which synapses convey specific information content to neurons and provide synaptic drive to initiate spike firing, whereas intrinsic plasticity affects the ability of a neuron to influence signal propagation within its respective neural circuit, possibly in the absence of accompanying changes in synaptic weight (see Titley et al., 2017).

## METHODS

All methods can be found in the accompanying Transparent Methods supplemental file.

## SUPPLEMENTAL INFORMATION

Supplemental Information includes Transparent Methods and can be found with this article online at https://doi.org/10.1016/j.isci.2018.02.001.

## AUTHOR CONTRIBUTIONS

G.O. and C.H. designed the experiments. G.O. performed the experiments. G.O. and C.H. analyzed the data and wrote the paper.

## DECLARATION OF INTERESTS

The authors declare no competing interests.

## REFERENCES

Aizenman, C.D., and Linden, D.J. (1999). Regulation of the rebound depolarization and spontaneous firing patterns of deep nuclear neurons in slices of rat cerebellum. J. Neurophysiol. 82, 1697–1709.

Alvina, K., Walter, J.T., Kohn, A., Ellis-Davies, G.C., and Khodakhah, K. (2008). Questioning the

role of rebound firing in the cerebellum. Nat. Neurosci. 11, 1256–1258.

Belmeguenai, A., Hosy, E., Bengtsson, F., Pedroarena, C.M., Piochon, C., Teuling, E., He, Q., Ohtsuki, G., De Jeu, M.T., Elgersma, Y., et al. (2010). Intrinsic plasticity complements long-term potentiation in parallel fiber input gain control in

cerebellar Purkinje cells. J. Neurosci. 30, 13630–13643.

Cingolani, L.A., Gymnopoulos, M., Boccaccio, A., Stocker, M., and Pedarzani, P. (2002). Developmental regulation of small-conductance Ca2+ -activated K+ channel expression and function in rat Purkinje neurons. J. Neurosci. 22, 4456–4467.

De Ruiter, M.M., De Zeeuw, C.I., and Hansel, C. (2006). Voltage-gated sodium channels in cerebellar Purkinje cells of mormyrid fish. J. Neurophysiol. *96*, 378–390.

De Schutter, E. (1998). Dendritic voltage and calcium-gated channels amplify the variability of postsynaptic responses in a Purkinje cell model. J. Neurophysiol. *80*, 504–519.

Dykstra, S., Engbers, J.D., Bartoletti, T.M., and Turner, R.W. (2016). Determinants of rebound burst responses in rat cerebellar nuclear neurons to physiological stimuli. J. Physiol. *594*, 985–1003.

Edgerton, J.R., and Reinhart, P.H. (2003). Distinct contributions of small and large conductance Ca2+ -activated K+ channels to rat Purkinje neuron function. J. Physiol. *548*, 53–69.

Grasselli, G., He, Q., Wan, V., Adelman, J.P., Ohtsuki, G., and Hansel, C. (2016). Activity-dependent plasticity of spike pauses in cerebellar Purkinje cells. Cell Rep. *14*, 2546–2553.

Hansel, C., Linden, D.J., and D'Angelo, E. (2001). Beyond parallel fiber LTD: the diversity of synaptic and non-synaptic plasticity in the cerebellum. Nat. Neurosci. *4*, 467–475.

Häusser, M., and Clark, B.A. (1997). Tonic synaptic inhibition modulates neuronal output pattern and spatiotemporal synaptic integration. Neuron *19*, 665–678.

Hosy, E., Piochon, C., Teuling, E., Rinaldo, L., and Hansel, C. (2011). SK2 channel expression and function in cerebellar Purkinje cells. J. Physiol. *589*, 3433–3440.

Larkum, M.E., Zhu, J.J., and Sakmann, B. (2001). Dendritic mechanisms underlying the coupling of the dendritic with the axonal action potential initiation zone of adult rat layer 5 pyramidal neurons. J. Physiol. *533*, 447–466.

Marder, E., Abbott, L.F., Turrigiano, G.G., Liu, Z., and Golowasch, J. (1996). Memory from the dynamics of intrinsic membrane currents. Proc. Natl. Acad. Sci. USA *93*, 13481–13486.

Ohtsuki, G., Piochon, C., Adelman, J.P., and Hansel, C. (2012). SK2 channel modulation contributes to compartment-specific dendritic plasticity in cerebellar Purkinje cells. Neuron *75*, 108–120.

Person, A.L., and Raman, I.M. (2012). Purkinje neuron synchrony elicits time-locked spiking in the cerebellar nuclei. Nature *481*, 502–505.

Piochon, C., Kloth, A.D., Grasselli, G., Titley, H.K., Nakayama, H., Hashimoto, K., Wan, V., Simmons, D.H., Eissa, T., Nakatani, J., et al. (2014). Cerebellar plasticity and motor learning deficits in a copy-number variation mouse model of autism. Nat. Commun. *5*, 5586.

Piochon, C., Kano, M., and Hansel, C. (2016). LTD-like molecular pathways in developmental synaptic pruning. Nat. Neurosci. *19*, 1299–1310.

Roth, A., and Häusser, M. (2001). Compartmental models of rat cerebellar Purkinje cells based on simultaneous somatic and dendritic patch-clamp recordings. J. Physiol. *535*, 445–472.

Sourdet, V., Russier, M., Daoudal, G., Ankri, N., and Debanne, D. (2003). Long-term enhancement of neuronal excitability and temporal fidelity mediated by metabotropic glutamate receptor subtype 5. J. Neurosci. *23*, 10238–10248.

Stuart, G., and Häusser, M. (1994). Initiation and spread of sodium action potentials in cerebellar Purkinje cells. Neuron *13*, 703–712.

Sun, Q., Srinivas, K.V., Sotayo, A., and Siegelbaum, S.A. (2014). Dendritic Na$^+$ spikes enable cortical input to drive action potential output from hippocampal CA2 pyramidal neurons. Elife *3*, e04551.

Telgkamp, P., and Raman, I.M. (2002). Depression of inhibitory synaptic transmission between Purkinje cells and neurons of the cerebellar nuclei. J. Neurosci. *22*, 8447–8457.

Titley, H.K., Brunel, N., and Hansel, C. (2017). Toward a neurocentric view of learning. Neuron *95*, 19–32.

Vetter, P., Roth, A., and Häusser, M. (2001). Propagation of action potentials in dendrites depends on dendritic morphology. J. Neurophysiol. *85*, 926–937.

Womack, M.D., and Khodakhah, K. (2003). Somatic and dendritic small-conductance calcium-activated potassium channels regulate the output of cerebellar Purkinje neurons. J. Neurosci. *23*, 2600–2607.

# Supplemental Information

# Synaptic Potential and Plasticity of an SK2

# Channel Gate Regulate Spike Burst

# Activity in Cerebellar Purkinje Cells

Gen Ohtsuki and Christian Hansel

**Transparent Methods**

*Animals and slice preparation*

Sagittal slices of the cerebellar vermis (220μm thick) were prepared from P25-37 Sprague-Dawley rats after isoflurane anesthesia and decapitation. The procedure is in accordance with the guidelines of the Animal Care and Use Committee of the University of Chicago. Slices were cut on a vibratome (Leica VT1000S) using ceramic blades. Slices were kept in ACSF containing the following (in mM): 124 NaCl, 5 KCl, 1.25 $Na_2HPO_4$, 2 $MgSO_4$, 2 $CaCl_2$, 26 $NaHCO_3$ and 10 D-glucose, bubbled with 95% $O_2$ and 5% $CO_2$.

*Patch-clamp recordings*

The recordings were performed in a recording chamber superfused with ACSF at near-physiological temperature (31-34°C). The ACSF was supplemented with 100μM picrotoxin to block $GABA_A$ receptors. Somato-dendritic double-patch recordings were performed under visual control using differential interference contrast optics in combination with near-infrared light illumination (IR-DIC) using a Zeiss AxioCam MRm camera and a x40 IR-Achroplan objective, mounted on a Zeiss Axioscope 2FS microscope (Carl Zeiss MicroImaging). Patch-clamp recordings were performed in current-clamp mode (Rs compensation off / fast capacitance compensation on) using an EPC-10 quadro amplifier (HEKA Electronics). Membrane voltage and current were filtered at 3kHz, digitized at 25kHz, and acquired using Patchmaster software. We used patch pipettes pulled from borosilicate glass for both the dendritic and somatic recordings, which were filled with a solution containing (in mM): 9 KCl, 10 KOH, 120 K-gluconate, 3.48 $MgCl_2$, 10 HEPES, 4 NaCl, 4 $Na_2ATP$, 0.4 $Na_3GTP$, and 17.5 sucrose (pH 7.25). The membrane voltage was corrected for liquid junction potentials (11.7mV). Dendritic patch electrodes had electrode resistances of 7-10MΩ, while the somatic patch electrodes had electrode resistances of 2-5MΩ. Hyperpolarizing bias currents (100-350pA) were injected to stabilize the membrane potential at about -75mV and to prevent spontaneous spike activity that would interfere with the analysis of evoked spiking. For PF stimulation (1-8μA / 200μs pulses), glass pipettes were placed in the molecular layer. Trains of five stimuli were applied at 50Hz to obtain trains of EPSPs with rising amplitude. It should be noted that application of the synaptic activation pattern from a holding potential of ~ -75mV does not faithfully mimic synaptic activation and spike initiation under physiological conditions. However, it is important to perform these recordings in the absence of confounding spontaneous spike

activity, which made it necessary to inject bias currents. We adjusted the EPSP amplitude such that at least EPSP 5 would be able to evoke spike firing. This strategy allowed us to probe for the efficiency of EPSP amplitude and intrinsic excitability, respectively, in triggering spikes and spike bursts, while only permitting evoked spike activity. In the presence of spikes, the EPSP amplitude was measured as the amplitude of the slow response component. The AHP amplitude was determined by measuring the negative peak. Three cells were excluded from the AHP analysis, because of problems with the AHP measure (spike activity and one outlier value, respectively). For tetanization, we used PF burst stimulation (50Hz; 5 pulses), or injection of depolarizing currents (300-400pA / 100ms), both at 5Hz for 3-4s. In the test periods before and after tetanization, the EPSPs were not continuously monitored, but acquisition of PF responses was restricted to the baseline and the end of the recordings, 20min after tetanization.

*Data analysis*

The data shown here result from an extended analysis of recordings presented in a published study (Ohtsuki et al., 2012). Data were analyzed using Fitmaster software (HEKA Electronics) and Igor Pro software (WaveMetrics). Statistical significance was determined by using the paired Student's t test (to test for significance of changes after an experimental manipulation in comparison to baseline) and the Mann-Whitney U test (between-group comparison), when appropriate. Spearman's rank correlation coefficient ρ was calculated to determine whether or not there were monotonic (progressively increasing / decreasing; no linearity needed) correlations between the amplitude of EPSP 5 or the AHP / spike threshold, respectively, and the spike output, organized in the ordinal categories 'no spike', 'one spike', 'weak burst' (2 spikes) and 'strong burst' (3-6 spikes). All data are shown as mean ± SEM.